AIMS Biophysics

AIMS Biophysics, 8(2): 124–142.
DOI: 10.3934/biophy.2021010
Received: 26 December 2020
Accepted: 04 March 2021
Published: 10 March 2021

http://www.aimspress.com/journal/biophysics

Research article

Radioprotective effect of nanoceria and magnetic flower-like iron oxide microparticles on gamma radiation-induced damage in BSA protein

Running Title: Radioprotective Effect of Nanostructures on BSA

Mostean Bahreinipour[1], Hajar Zarei*[,2,3], Fariba Dashtestani[4], Jamal Rashidiani[5], Khadijeh Eskandari[5], Seyed Ali Moussavi Zarandi[1], Susan Kabudanian Ardestani[4] and Hiroshi Watabe*[,3]

[1] Department of Energy Engineering and Physics, Faculty of Physics, Amirkabir University of Technology, Tehran, Iran
[2] Persian Gulf Research Institute, Persian Gulf University Bushehr, Iran
[3] Cyclotron and Radioisotope Center (CYRIC), Tohoku University, Sendai, Miyagi, Japan
[4] Institute of Biochemistry & Biophysics, University of Tehran, Tehran, Iran
[5] Nanobiotechnology Research Center, Baqiyatallah University of Medical Science, Tehran, Iran

* **Correspondence:** Email: HajarZarei@pgu.ac.ir, watabe@cyric.tohoku.ac.jp; Tel: +810227957800; Fax: +810227957803, +810227957809.

Abstract: *Purpose:* Gamma radiation at therapeutic doses can cause conformation changes in proteins and consequently damage cells/tissues associated with the initiation of several pathological disorders. In this study, serum albumin, the most abundant protein in plasma, was chosen as the protein sample. *Methods and Materials:* Bovine serum albumin (BSA) was exposed to gamma radiation at a therapeutic dose (3 Gy) in the absence and presence of Ceria nanoparticles (CNPs) and flower-like Fe_3O_4 microparticles (FIOMPs). The conformational changes in BSA including primary, secondary, tertiary structures were then studied by UV-Vis, circular dichroism (CD), and fluorescence spectroscopy, respectively.
Results: The primary structure of gamma-irradiated BSA (IR-BSA) was conserved, whereas the secondary and tertiary structures were considerably changed. IR-BSA showed α-helix to β-sheet and random coil structure transition along with reduced fluorescence emission intensity compared to non-irradiated native BSA. Both CNPs and FIOMPs could inhibit the secondary and tertiary structural changes in IR-BSA by scavenging the reactive oxygen species produced during the radiolysis of water. *Conclusions:* The radioprotective property of CNPs arises from enzyme mimetic

activities (catalase, superoxide dismutase, and peroxidase) and their antioxidant capability against hydroxyl radicals. In case of FIOMPs, the radioprotective property is attributed to catalase mimetic activity (CAT), and a porous structure leading to increased ROS recombination with each other in the same radiolytic track, and subsequently decreased encounters with BSA. The latter mechanism of restricting ROS migration seems to be more dominant for FIOMPs. Both CNPs/FIOMPs themselves at low concentrations do not show a significant effect on the native protein conformation. These findings indicate that the proposed NPs/MPs can be good candidates for developing strong nano-radioprotectors.

Keywords: bovine serum albumin; gamma radiation; spectroscopy; ceria nanoparticles; flower microparticles; nano-radioprotector

1. Introduction

Radiation therapy is an effective approach to control and cure malignant cancer. However, normal cells surrounding the tumor inevitably receive a considerable dose of ionizing radiation, resulting in their damage. Although the total advantages of radiation therapy exceed its side effects, recent studies have focused on alleviating radiation damage to surrounding healthy cells [1–2]. The damaging effects of ionizing radiations on cells/tissues result from two mechanisms; i) direct damage through interaction/hitting on molecules within cells such as, direct effects on DNA, RNA, and proteins, resulting in disruption of the molecular structure [3], ii) indirect effects through interact with cellular water as an intermediate step and generation of reactive oxygen species (ROS) including free radicals and non-radical oxidizing agents (hydrogen peroxide (H_2O_2), H_2). These ROS in turn interact with cellular atoms and molecules resulting in their chemical modification and consequent harmful effects [4–5].

Proteins are important biomolecules that play significant roles in living organisms. The chemical changes induced by gamma irradiation in proteins lead to structural changes, fragmentation, cross-linking, aggregation, changes in protein electrical charge, and oxidation. It is thus responsible for the initiation or progress of several pathological disorders (cancer, neurodegenerative diseases, inflammatory diseases, etc.) [6–9]. Among mammalian proteins, serum albumin is one of the most vital and abundant protein in plasma, possessing many physiological roles such as a plasma carrier for transporting various hormones, fatty acids, different drugs, bilirubin, and vitamins from the blood stream to tissues [10–11]. Bovine serum albumin (BSA), which has more than 76% similarity with human serum albumin (HSA), is stable, biocompatible, and readily available at a very low cost compared to HSA [12]. Therefore, BSA is widely studied. It is a single-chain protein of 583 amino acids with a molecular weight of 66 k Da with two tryptophan (Trp), 19 tyrosine (Tyr), and 27 phenylalanine (Phe) amino acid residues that contribute to its intrinsic fluorescence intensity [8,13–14]. H. Schuessler et al, have reported that irradiated BSA is cleaved by the oxidative destruction of proline residues [15]. Hu et al. have reported that the conformation of HSA subjected to gamma irradiation was changed, its esterase-like activity was reduced, and the content of bi-tyrosine was increased because of oxidation by the generated ROS [16]. BSA protein exposed to gamma rays at a therapeutic dose (3 Gy) showed disturbed conformation, but no fragmentation, cross-linking, or aggregation were observed [17].

With respect to the potential application of ionizing radiation in radiotherapy and medical diagnostic exposures, the development of effective radio protective agents such as antioxidant supplements are highly desired to reduce oxidative damage to proteins and other biomolecules [9]. To date, vitamin C [18], vitamin E [19], ferulic acid [20], wheat germ oil, ginseng extract [21], and extract of piper betel [22] have been frequently studied and applied as common natural radio-protectors. Although natural antioxidants have low toxicity, they have limitations of low aqueous solubility, lack of specificity, and poor bioavailability (ease of metabolism). Recently, synthetic nanostructures have attracted much attention as nano radioprotectors to overcome these limitations. Nanoparticles can provide higher solubility to poorly water-soluble compounds, resistance to digestion by proteases, and enhanced surface functionalization to yield target-specificity [23]. In literature, nano-radioprotectors are called antioxidant nano-enzymes abbreviated as Nanozymes. Among these nanostructures, silver, gold, cerium oxide, Fe_3O_4 nanoparticles, and carbon nanotubes have been used frequently [24]. Colon et al. [25] have reported that ceria nanoparticles (CNPs) protect radiation-induced damage *in vitro* and *in vivo*. CNPs possess long-lasting antioxidant properties, due to the auto generation of $Ce^{3+}\leftrightarrow Ce^{4+}$ on their surface with respect to valence and oxygen vacancies, thus promoting free radical scavenging [26]. Ferro magnetite (Fe_3O_4) nanoparticles have antioxidant effects with intrinsic dual peroxidase-catalase activities and can thus reduce H_2O_2 in biological systems [27–28]. Several studies have investigated the effect of natural and nano radio-protective nanostructures on DNA fragmentation but very few studies have examined protein damage [20,23].

In this study, the radio-protective effect of synthesized CNPs and magnetic flower-like Fe_3O_4 microparticles (FIOMPs) on irradiated BSA was investigated. For this purpose, BSA, in the presence and absence of nanostructures, was exposed to a therapeutic dose of gamma radiation (3 Gy). The structural and surface charge changes in BSA were studied using spectroscopic methods including UV-Vis, florescence, and CD spectroscopy. To our knowledge, this is the first direct study to investigate the antioxidant and radio-protective properties of nano/microparticles such as CNPs and FIOMPs in the inhibition of radiation damage to BSA as a protein sample. Considering the major role of albumin as a drug and hormone carrier, this study has implications in the pharmaceutical studies on irradiated albumin in the presence of nano-radioprotectors to evaluate their functionality.

2. Materials and experimental

2.1. Materials

BSA, potassium dihydrogen phosphate (KH_2PO_4), potassium hydrogen phosphate (K_2HPO_4), ammonium cerium (IV) nitrate [$(NH_4)_2Ce\ (NO_3)_6$], sodium acetate [CH_3COONa], and acetic acid [CH_3COOH] were purchased from Merck (Germany) and were used without further purification. Ferric chloride ($FeCl_3\ 6H_2O$), urea, tetrabutylammonium bromide (TBAB), ethylene glycol, and sodium dodecyl sulfate (SDS) were purchased from Sigma chemical company (USA). Formic acid was obtained from Chem-Lab (USA). The solutions were prepared in deionized double distilled water (Barnstead, Nano pure infinity, USA) and all experiments were carried out at room temperature.

2.2. Apparatus

UV-Vis spectra were recorded using a Cary 100 Bio spectrophotometer (Varian, Australia). Fluorescence and CD spectra were obtained using spectrofluorometers of model MPF-4 (Hitachi, Japan) and model 215 (Aviv, USA), respectively. Scanning electron microscopy images were obtained using field emission scanning electron microscopy (FESEM) on model S4160 (Hitachi, Japan).

2.3. Synthesis of CNPs and FIOMPs

CNPs were synthesized based on a hydrothermal method as described previously [29]. Briefly, 2.74 g of ceric ammonium nitrate and 10 g of sodium acetate were dissolved in 70 ml of deionized water; then, 10 ml of acetic acid was added to the solution and stirred at room temperature for 1 h. The mixture was then transferred to a Teflon-lined autoclave for hydrothermal treatment at 220 ℃ for 12 h. Finally, to eliminate the remaining salt, the yellow precipitates were separated by centrifugation (6,000 × g) for 10 min, washed several times with deionized water and ethanol, and air-dried overnight at 60 ℃.

The 3D nanostructure of FIOMPs was synthesized using the method described by Zhong et al. [30]. Briefly, ferric chloride ($FeCl_3$ $6H_2O$), urea, and tetrabutylammonium bromide (TBAB), were dissolved in ethylene glycol. The solution was incubated at 200 ℃ for 30 min. After cooling, the green precipitate of synthesized iron oxide was collected by centrifugation and washed with ethanol. The morphology of FIOMPs was then studied using FESEM.

2.4. Sample preparation and gamma irradiation

The BSA solution was prepared in 10 mM PBS (pH 7.0) with a final concentration of 0.4 mg/mL. Samples containing either CNPs or FIOMPs were prepared in the BSA solution at various concentrations (0, 2, 5, 8, 12, 20, and 25 mg/L). The prepared BSA solutions with and without CNPs or FIOMPs were irradiated at room temperature using a ^{60}Co gamma ray irradiator (Theratron 780-E, Canada) at Imam Khomeini hospital (Iran, Tehran). The radiation absorbed dose in each sample was 3 Gy, obtained by 1 min of irradiation. The field of view (FOV) and source skin distance (SSD) of irradiation were 25 cm × 25 cm and 80 cm, respectively. The glass vials containing the protein samples were placed in a large water pool made of plexiglass to obtain electron balance in the wall of the glass vials during irradiation. The water pool dimension was 20 × 20 × 10 cm^3. The plexiglass container was placed in the front of ^{60}Co source at the center of the FOV.

3. Results

3.1. Characterization of CNPs and FIOMPs

As shown in Figure 1 (A and B), the FESEM images reveal that the CNPs are spherical with a diameter less than 50 nm and that the core thickness of FIOMPs is 2 μm with petals of 50 nm in size. According to the procedure used, only the Fe_3O_4 form of iron oxide was obtained in our experiment by the partial reduction of Fe (III) [30].

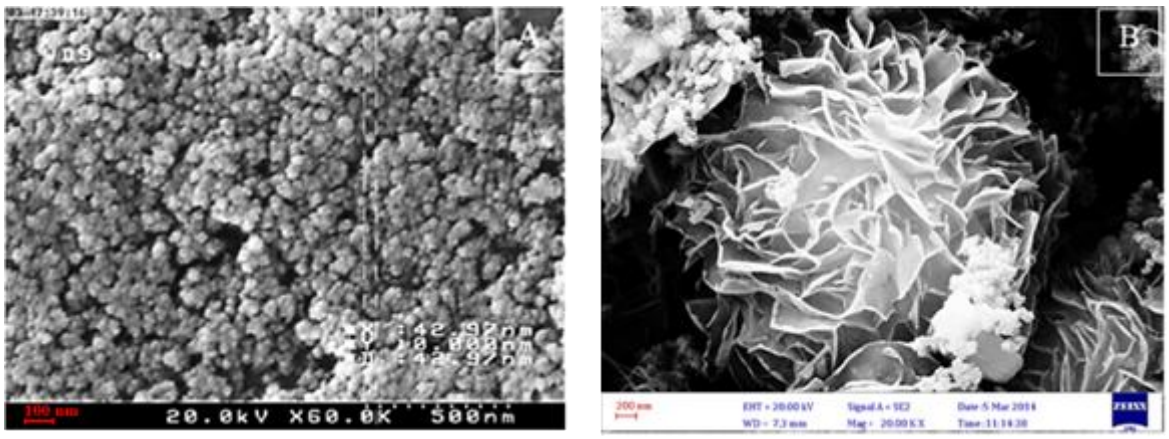

Figure 1. FESEM images of CNPs (A) and FIOMPs (B) at a magnification of 60 K and 20 K, respectively.

3.2. UV–vis spectroscopy

The UV-vis absorption spectra of native BSA and IR-BSA show two maximum peaks, the peak around 220 nm (far-UV) indicates the $n \rightarrow \pi^*$ transition in the polypeptide backbone, and the other at 280 nm indicates the $\pi \rightarrow \pi^*$ transfer in the side chain of aromatic amino acids, Trp, Tyr, and Phe (Figure 2). Disturbance of the local environment around the amino acids residues, leading to changes in the backbone and side chain of aromatic amino acids, can change the intensity and position of the first and second peak, respectively. Thus, conformational changes in protein structures may be accompanied with protein unfolding [9,31]. An increase in absorbance at the 280 nm peak is observed after protein irradiation, indicating changes in the microenvironment of the aromatic amino acids and subsequently in the protein conformation, though no difference is seen at the 220 nm peak. However, the change in UV-Vis spectroscopy due to irradiation at an especially high dose could also be attributed to the cleavage of the covalent bonds in the peptide backbone and aggregation resulting in a decrease and increase in the protein molecular weight, respectively [12]. The aggregation index of native BSA and IR-BSA was calculated using Eq. 1 as below [32]:

$$\text{Aggregation index} = \frac{\text{Abs350}}{\text{Abs280}-\text{Abs350}} \quad (1)$$

Where Abs350 and Abs280 represent the absorbance (%Abs) at 350 nm and 280 nm, respectively. The calculated aggregation index value was about 3 and 2.7 for native BSA and IR-BSA, respectively indicating that there was no aggregation after irradiation treatment [32]. Overall, the results of UV-Vis spectroscopy confirm no protein cleavage or aggregation, which is contrary to the results reported by Gaber et al. [12].

Techniques such as sodium dodecyl sulfate-polyacrylamide gel electrophoresis (SDS-PAGE), high performance liquid chromatography (HPLC), and dynamic light scattering (DLS) are commonly used to determine protein molecular weight [12,17]. In our previous work using SDS-PAGE and HPLC techniques, we found that the molecular weights of native BSA and IR-BSA are the same and that the backbone (primary structure) of BSA protein is completely preserved [17]. Radiation can change protein structure directly as well as indirectly through ROS produced during water radiolysis.

However, our results indicate that both the direct and indirect effects of gamma-radiation were ineffective to break the peptide bond in the protein or to cause significant unfolding resulting in its aggregation.

Direct cleavage of the protein backbone due to gamma irradiation was impossible due to the insufficient energy of the applied therapeutic dose compared to that used by Gaber et al. [12]. The indirect effect of gamma radiation can be explained by the ratio of the number of ROS products of water radiolysis to the number of protein molecules. This simple estimation was calculated based on the applied dose and the radiolytic yields (μmol J^{-1}) of species produced in water by low LET gamma rays (Table 1) [33]. The OH•, H_2O_2, and O_2•−/HO_2• to BSA ratio in this work was approximately 0.13, 0.03, and 0.001, respectively. In the study by Gaber et al., these ratios were approximately 23 and 6 for OH and H_2O_2, respectively. Thus, in this work, the number of ROS species was 1 to 3 orders of magnitude less than BSA, which seems insufficient to cause significant damage to the primary structure.

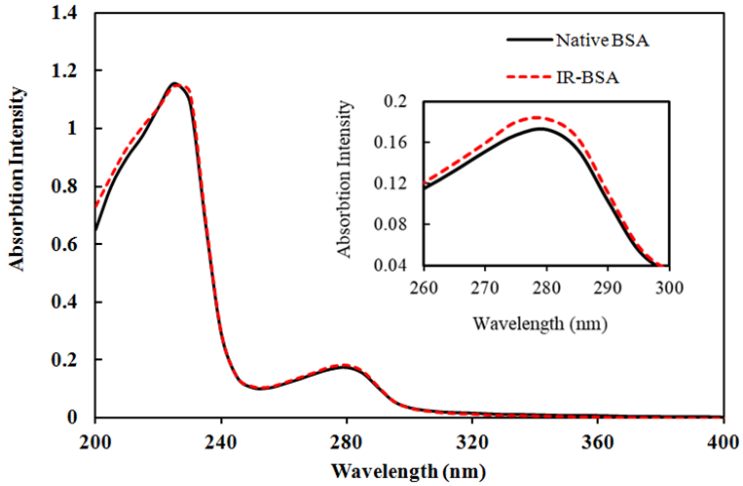

Figure 2. UV-Vis absorption spectra of native BSA (line) and IR-BSA (dash) at 3 Gy. The BSA concentration was 0.4 mg/mL in 10 mM PBS, pH = 7 at room temperature. The Inset is a close-up of the Region Between 260–300 nm.

Table 1. Radiolytic yields (μmol J^{-1}) of species produced in water by Low LET gamma rays [33].

Radiation	e^-_{aq}	$OH^•$	$H^•$	H_2	H_2O_2	O_2•−/$HO_2^•$
Gamma rays						
PH = 3–11	0.28	0.28	0.06	0.047	0.073	0.0027

3.3. CD spectroscopy

Both MPs/NPs and gamma rays can act as agents to cause conformational changes in BSA protein [12,34–37]. As these MPs/NPs are introduced as radioprotective agents, it is important that their effects on the protein conformational should be negligible or at least less than the destructive effect of radiation. Therefore, before investigating the radioprotective properties of NPs and MPs, it is necessary to appraise their effects on the protein conformation in the absence of gamma ray irradiation due to the direct interaction between them. Accordingly, the secondary and tertiary structures of BSA

at different concentrations of CNPs and FIOMPs were studied and compared with the native protein using far-UV CD and fluorescence spectroscopy, respectively.

The molar ellipticity of native BSA and IR-BSA solutions in the presence of various concentrations of CNPs and FIOMPs (0 to 25 mg/L) was measured between 190 to 260 nm (Supplement Data Figure 1S and 2S). The far-UV CD spectra of BSA exhibited a signal characteristic of the α-helix structure with two negative bands in the far-UV region at 208 nm and 222 nm [38], because of the contribution of the $n \rightarrow \pi^*$ transfer to the peptide bond in the α-helix [8]. The proportion of the secondary structure contents of BSA calculated by the algorithm CDNN2.1 [39–40] in the presence of CNPs and FIOMPs are shown in Figure 3 (A and B) and Figure 4 (A and B), in which each of the secondary structure contents are normalized to a total content of 100% by the deconvolution of CD spectra. The error bars are the standard errors of the mean (SEM) for five measurements and are less than 5%, confirming the reliability of the data. The reproducibility of the CD analysis for native BSA (Mean ± SD, n = 5) showed that it contains 59.5 ± 2.5% α-helix, 8.5 ± 2% β-sheets, 13.5 ± 1.2% turns, and 19 ± 1.5 random coils. These values were also calculated for IR-BSA and showed 54.5 ± 3.5% α-helix, 9.75 ± 1.5% β-sheets, 14.75 ± 1.2% turns, and 21 ± 2.5 random coils.

To confirm that there were no significant differences in the secondary structures between the Native-BSA and IR-BSA treated with different concentration of CNPs or FIOMPs, an unpaired t-test was performed using SPSS version 16. We thus classified our data into three main groups: all measurements for each secondary structure of Native-BSA in the absence of NPs or MPs (group 1), Native-BSA (group 2), and IR-BSA (group 3) treated with NPs or FIOMPs, for example, at 2 mg/L. Two separate t-tests were calculated to compare group 1 and group 2 (Figure 3 and 4 A) as well as group 1 and group 3 (Figure 3 and 4 B). A p-value less than 0.05 (*) indicated that the difference was statistically significant whereas values greater than 0.05 indicated that the difference was not statistically significant; thus, the corresponding NPs concentration was selected as the optimal nano-radioprotector concentration. The results showed no significant effect on the secondary structure of BSA at concentrations less than 5 mg/L of CNPs and at wide range of 5 to 20 mg/L FIOMPs. With the increase in CNPs from 8 to 25 mg/L, the protein showed an almost constant 6% loss of α-helix content with a corresponding 1.5% and 2–3% increase in β-sheet and random structures, respectively, along with unfolding (p-value < 0.05) at low and high MFMP concentrations (2 and 25 mg/L). No concentration dependency was observed with FIOMPs for a broad range, contrary to what was found for CNPs.

The α-helix content in IR-BSA (without CNPs or FIOMPs) decreased around 7% and the β-sheet and random coil increased by around 1% and 2%, respectively, compared to native BSA (p-value < 0.001). This secondary structure disruption was attributed to the interaction between the ROS produced by radiolysis of water and the protein [17]. The secondary structural contents of IR-BSA in the concentration range of 2–5 mg/L for CNPs and from 5–20 mg/L for FIOMPs were approximately the same as those in Native-BSA (p-value > 0.05) indicating remarkable protection from the destructive effect of ROS produced by gamma rays. The optimum range indicated that there was no disruptive effect on the de-conformation of the native protein and that ROS species were also hindered from attack the protein effectively with their scavenging activity. The significant difference between Native and IR-BSA at CNP and MFMP concentrations less than the optimum was due to the insufficient concentration for scavenging all the produced ROS and the unfolding effect as well as insufficient concentration, respectively. However, the altered content of secondary structures at concentrations greater than the optimum was attributed to the disturbing effect of NPs and MPs. The results for both

NPs and MPs showing an optimum concentration range instead of an optimum point are beneficial for future applications as a slight fluctuation in concentration would not cause a significance effect on their radioprotection activity.

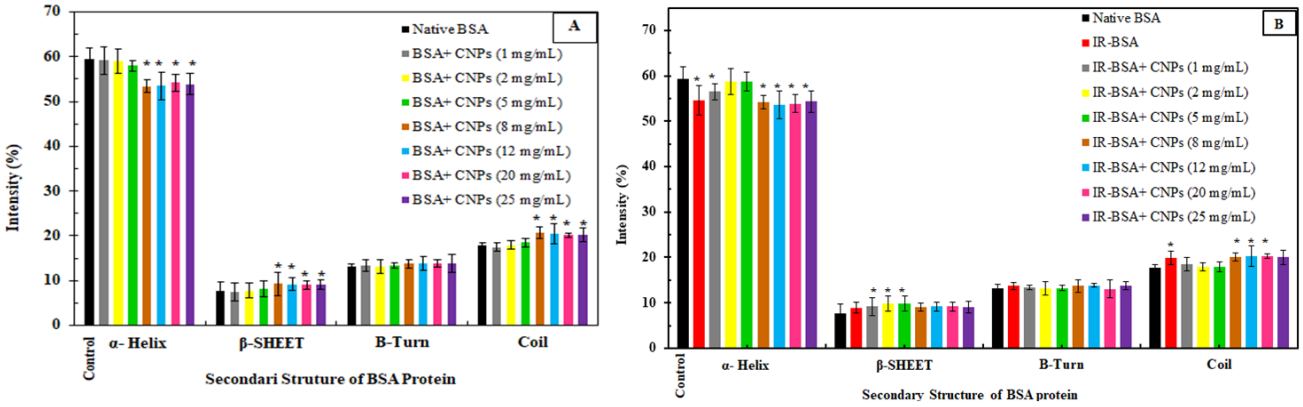

Figure 3. Secondary structural content of (A) BSA, and (B) IR-BSA by gamma rays (3 Gy) in the presence of various concentrations of CNPs obtained from the deconvolution of CD spectra in the far-UV region (190–260 nm) using the deconvolution software CDNN2.1. The error bars are the standard errors (SEM) of the five measurements and are less than 5% confirming the data reliability. The * sign indicates a p-value < 0.05 and a statistically significant difference. BSA indicates the non-irradiated protein treated with CNPs. The 0.4 mg/mL BSA was prepared in 10 mM PBS (pH 7.0) solutions.

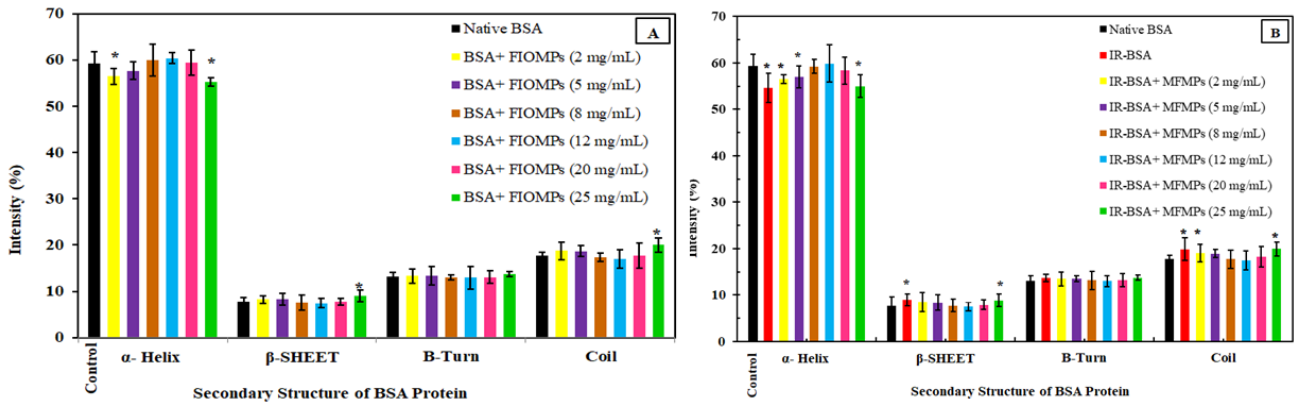

Figure 4. Secondary structural content of (A) BSA and (B) IR-BSA by gamma rays (3 Gy) in the presence of various concentrations of FIOMPs obtained with the same method as for Figure 5.

3.4. Fluorescence spectroscopy

Changes in the tertiary conformation of the protein can be determined from by fluctuations in the tryptophan fluorescence [7–8]. Fluorescence spectroscopy evaluates conformational changes around Trp residues as the dominant source of intrinsic protein fluorescence [35–41]. The fluorescence emission for BSA was recorded from 300 nm to 440 nm with λ_{ex} = 280 nm, and the

maximum peak fluorescence was found at 345 nm. The maximum fluorescence emission intensity of native BSA and IR-BSA in the presence of different concentrations of CNPs and FIOMPs is shown in Figure 5 and Figure 6, respectively (the average corresponding fluorescence spectra are shown in supplementary data Figure 3S and 4S, respectively.

The results show that that both CNPs and FIOMPs have a quenching effect on BSA fluorescence, with the same behavior. This effect increases considerably by increasing the concentration of these nanomaterials. As observed, gamma-irradiation caused a significant decrease in the emission intensity of native BSA in the absence of CNPs and FIOMPs. Fluorescence spectroscopy is a strong and inherently more sensitive method than UV-Vis spectroscopy. Thus, the difference in the revealed fluorescence emission intensity between native and irradiated BSA was more significant than that revealed by UV absorption peak at 280 nm.

The fluorescence intensity of IR-BSA at concentrations lower than 12 mg/mL of both CNPs and FIOMPs was more than that of IR-BSA in their absence, but was slightly reduced compared to that of native BSA. The relatively significant quenching effect observed for IR-BSA was amplified at concentrations greater than 12 mg/mL of CNPs whereas it was not substantial for FIOMPs. According to the results of both secondary and tertiary protein structures, the optimum concentration ranges of CNPs and FIOMPs that could effectively protect the secondary and tertiary structures of BSA protein in the presence of ionizing gamma rays were 2–5 mg/mL and 5–8 mg/mL, respectively. The fluorescence intensity of BSA treated with CNPs or FIOMPs before and after irradiation was almost the same. This confirmed the scavenging of ROS species by CNPs/FIOMPs although their emissions even at optimum concentrations were somewhat less than those of native BSA.

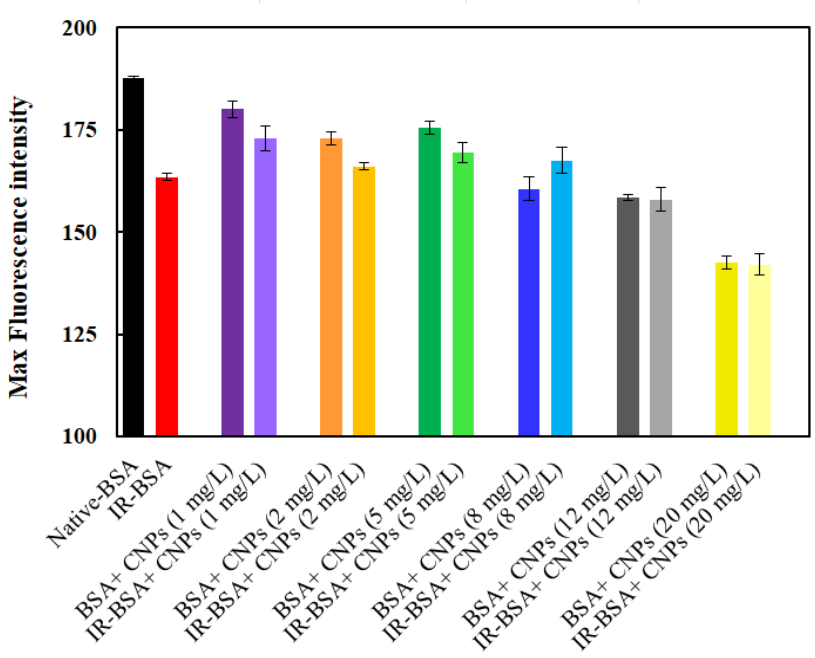

Figure 5. Fluorescence emission spectra of native BSA and IR-BSA by gamma rays (3 Gy) treated with different concentrations of CNPs. The solutions of 0.4 mg/mL BSA in 10 mM PBS (pH 7.0) were excited at 280 nm and the emission spectra were recorded from 300 to 440 nm.

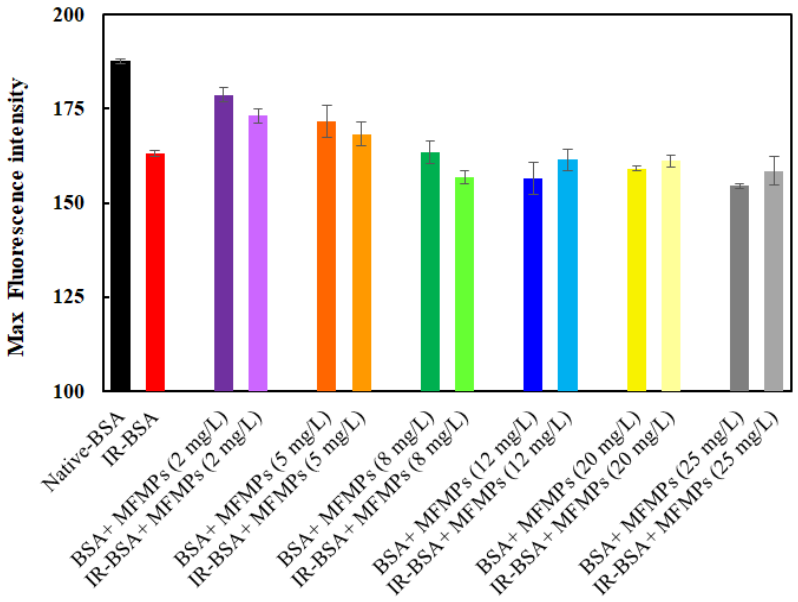

Figure 6. Fluorescence emission spectra of native BSA and IR-BSA by gamma rays (3 Gy) treated with different concentrations of FIOMPs. The experiment conditions were the same as those used in Figure 5.

3.4.1. Measurements of affinity between BSA and MPs/NPs using fluorescence spectroscopy

To further clarify and quantify the mechanism of quenching of BSA by MPs or NPs, the quenching constant and binding parameter were calculated using the fluorescence measurements of BSA in the presence of different concentrations of MPs or NPs as reported in the previous section. The peak fluorescence emission at 354 nm was determined to calculate the parameters. The fluorescence quenching data were then analyzed using the Stern–Volmer Eq. 2 shown below [42]:

$$\frac{F_0}{F} = K_{SV}[Q] + 1 \tag{2}$$

Where F_0 and F are the steady-state fluorescence intensities in the absence and presence of the quencher, respectively, K_{SV} is the Stern-Volmer quenching constant and [Q] is the concentration of the quencher [MPs or NPs]. The linearity of the F_0/F versus [Q] plots is shown in supplementary Figure 5S and K_{SV} is calculated from the slope of the plot.

The binding constant (K) and number of binding sites (n) between CNPs and FIOMPs with BSA can be calculated using Eq. 3 for the quenching process [42]:

$$\log[\frac{F_0\text{-}F}{F}] = \log K + n \log[Q] \tag{3}$$

A plot of log $[(F_0\text{-}F)/F]$ versus log [Q] gives a straight line (supplementary data Figure 6S), whose slope equals n and the intercept on Y-axis equals log K.

The values of K_{SV}, K, and n have been listed in Table 2. The values of n approximately equal to 1

indicate the existence of a single binding site on BSA for both CNPs and FIOMPs, which are prone to adsorb non-polar amino acids onto their surface. Comparison between two radio-protective particles indicated that the CNPs have a greater quenching effect and binding constant value compared to the FIOMPs.

Table 2. Binding parameters of BSA-CNP and BSA-MFMP interactions at room temperature

Interaction	K_{SV} (M^{-1})	K (M^{-1})	n
BSA- CNPs	3461	200	1
BSA- MFNPs	2710	107	1

Stern–Volmer quenching constant (K_{SV}), binding constant (K), and the number of binding sites (n)

4. Discussion

The spectroscopy results showed a preserved primary structure of the protein whereas damage to the secondary and tertiary structures in therapeutic range of irradiation (3 Gy), which indicated the indirect effect of gamma rays by producing ROS species. These structural modifications have different impacts on the functions of BSA as a drug carrier. They can thus be expected to affect its pharmacokinetic parameters, especially drug binding parameters [43].

4.1. Secondary structures

In general, both gamma-radiation and nanomaterials can alter the secondary and consequently, tertiary structures of a protein resulting in its unfolding and exposure of non-polar groups that were previously hidden within the core to the solvent. The reason for the α-helix transition to random coil and β-turn by radiation might be the cleavage of induced hydrogen bonds that destabilize the helix structure due to reactive oxygen species, so that unfolded structures are increased. Notably, low-dose radiation (3 Gy) caused partial unfolding (the limited α-helix transition), because it probably could not induce a high concentration of ROS species to destabilize all the existing hydrogen bonds [34]. The types and yields of ROS produced in water radiolysis by low LET ionizing radiation like gamma rays can be displayed below (Eq. 4) and in Table 1, respectively. As observed, the $OH^{\bullet}$ radical has a high yield among produced ROS and is a very strong oxidative species. H_2O_2 is also considered, though its yield and oxidant power is less than that of $OH^{\bullet}$. Thus, scavenging of these ROS species, especially $OH^{\bullet}$ and H_2O_2, is important to preserve protein conformation [33].

$$H_2O_2 \xrightarrow{\text{Ionization}} e^-_{aq},\ OH^{\bullet},\ H^{\bullet},\ O_2{\bullet}-,\ H_3O^+,\ OH^-,\ H_2O_2,\ H_2 \quad (4)$$

Two driving forces, protein-surface interaction and weak lateral interactions of proteins, can affect protein conformation (secondary and tertiary structural) adsorbed on NPs/MPs. The protein-surface interaction involves different bonding forces such as hydrogen bonds, solvation forces, Van der Waals interactions, and so on [44–45]. Changes in secondary structure depending on the CNP/MFMP concentration can be explained by the surface concentration (density) of the adsorbed BSA on their surface, called the "crowding effect." Regarding the same BSA concentration, the weak pro-pro and pro-surface interactions are the dominant forces at low and high NP/MP concentrations, respectively.

The weak pro-pro interactions result in the preservation of secondary structures and the subsequent functionality of the protein, whereas the pro-surface interactions disrupt protein folding. The larger surface obtained by increasing the MP/NP concentration provides larger interaction areas between the protein and particles leading to more secondary structure changes, consistent with the reported literature [46]. The generated coulombic forces between NPs and Protein due to their attachment can weaken, disrupt, and break the hydrogen bonding between the α-helices and β-sheets of a protein. This finally results in surface-driven modifications to the protein secondary structure and subsequently induces changes in its tertiary structure [36,47]. The protein density and subsequently, the total extent of weak pro-pro interactions on the surface of FIOMPs at 2 mg/L is rather high, leading to the formation of a strong total force that can that can finally yield a new arrangement of weak interactions in the native BSA. It thus seems the effect of lateral pro-pro interactions is dependent on protein density and may act as a double-edged sword as reported in the literature [48]. It is important in explore whether NPs or MPs are used as radioprotectors have no significant effect on the conformational change of the Pro sample. Thus, this is a beneficial aspect of FIOMPs that have no effect on the secondary structure of BSA at a wide concentration range, indicating that they do not exert any toxic side-effects before gamma-irradiation.

4.2. Tertiary structures

The tertiary conformational changes in proteins adsorbed on particles depend on the surface filling density, ionic strength, and pH and are affected by protein-protein interactions on the surface [46]. The fluorescence intensity of BSA exposed to CNPs/FIOMPs or gamma rays was reduced [Figure 5 A and B]. The same effect on BSA protein was due to the change in the local environment around tryptophan and tyrosine residues. Generally, tryptophan and tyrosine have a high quantum yield in the hydrophobic environment within the protein core, and consequently show high fluorescence intensity. In contrast, their quantum yield in a hydrophilic environment exposed to solvent decreases leading to low fluorescence intensity. Therefore, both gamma radiation and nanomaterials cause local environment changes around the tryptophan and tyrosine residues to be exposed to the solvent [35,41]. Taken together, the florescence and CD spectroscopy results and statistical analysis of CD spectroscopy results by CDNN2.1 indicate that the damage caused by gamma radiation partially unfolded the protein. This can cause a decrease in the colloidal stability of the protein, which in turn, increases the possibility of inter-molecular interaction resulting in increased β-structures under partial unfolding [49–50]. The partial unfolding of IR-BSA was also confirmed by DLS in our previous work, indicating that its hydrodynamic size is increased compared to that of native BSA [17].

These results confirmed the direct interaction between BSA protein and NPs/MPs. The intensity of conformational changes of absorbed protein on NPs/MPs, dependent on the surface filling density, is determined by the characteristics of the MPs/NPs, such as their size, shape, and surface properties [46]. To obtain conditions with negligible conformational changes in the protein in the presence of NPs/MPs before irradiation, optimization of characteristics dependent on MPs/NPs is important. This can be evaluated by quantifying the K_{SV}, K, and n parameters, but was beyond the purpose of this work; they can thus be investigated in a future comprehensive study. Further, although this direct binding causes partial conformational changes in the protein, it may amplify the radioprotection activity by a shielding effect [51]. The native BSA and IR-BSA treated with CNPs show an increased quenching effect than that with FIOMPs due to their greater quenching constant (Table 2).

Therefore, the BSA conformational changes caused by CNPs at concentrations greater than the optimum were even greater than those in IR-BSA in their absence, whereas these were nearly negligible for FIOMPs except at 25 mg/L.

4.3. Water radiolysis in heterogeneous systems at MP or NP/water interfaces

In heterogeneous systems like MP or NP/water interfaces, gamma rays deposit energy to both simultaneously, compared to bulk water with only water. The production yield and elimination of ROS species in radiolysis water can be influenced and modified in the presence of oxide surface (CNPs and FIOMPs) with respect to those occurring in bulk water [33]. The effects dependent on the surface can be evaluated in two aspects; 1) the anti-oxidant activity of CNPs and FIOMPs against the generated ROS species [52–54], and 2) the change in reaction (recombination) and diffusion of produced species during the chemical stage of water radiolysis that is directly influenced by the size and morphology (porosity) of the particles [33,55–56].

4.4. Radioprotection ability of CNPs/FIOMPs

In the biological system, antioxidant scavenging enzymes such as peroxidase, catalase (CAT), superoxide dismutase (SOD), glutathione reductase, and so on, protect the cells/tissues from damage induced by an excess of free radicals. The substrate of CAT and hydrogen peroxidase is H_2O_2 whereas superoxide radicals are substrates for SOD. Among inorganic antioxidants, CNPs are frequently reported to demonstrate activity mimicking natural enzymes such as Catalase, Superoxide dismutase (SOD), and Peroxidase. These antioxidant activities and their intensity is attributed to the coexistence of two forms, Ce^{3+}/Ce^{4+}, and their extent on the surface of CNPs, respectively. Cerium can shift between Ce^{4+} and Ce^{3+} states under oxidizing and reducing conditions by reversibly binding with oxygen on the surface. It results in the formation of oxygen defects in the crystal lattice that acts as a reactive site for free radical scavenging in a reversible reaction. The CNPs with a high ratio of the Ce^{3+}/Ce^{4+} state at the surface exhibit SOD mimetic activity, whereas a high ratio the Ce^{+4}/Ce^{+3} oxidation state leads to CAT mimetic activity [53–54,57]. In addition to enzyme mimetic activities for scavenging H2O2, CNPs have a special antioxidant activity to reduce hydroxyl radicals whereas there is no such natural enzyme [58]. The catalase, SOD, and HO• scavenging activities are shown in the following proposed mechanisms Eq. 5, 6, and 8 respectively [53–54,57–58];

CAT Activity $\quad Ce\ (IV) + 2H_2O_2 \leftrightarrow Ce\ (III) + 2H_2 + 2O_2 \quad (5)$

SOD Activity $\quad Ce\ (IV) + O_2\bullet- \rightarrow Ce\ (III) + O_2 \quad (6)$

$\quad Ce\ (III) + O_2\bullet- + 2H^+ \rightarrow Ce\ (IV) + H_2O \quad (7)$

$HO^{\bullet}$ scavenging $\quad Ce\ (III) + 2\ HO^{\bullet} \rightarrow H_2O + Ce\ (IV) \quad (8)$

This multi-functionality related to antioxidant properties introduces CNPs as a strong scavenger of produced ROS, especially of hydroxyl radicals ($HO^{\bullet}$) with the highest production yield and reactivity, and one of the strongest oxidants [59]. Accordingly, CNPs at a low concentration (2 mg/L) can scavenge almost all the produced ROS without meaningfully disturbing the protein conformation.

FIOMPs have an antioxidant effect with intrinsic dual peroxidase-catalase activity in reducing H_2O_2 in biological systems. The optimum conditions for the peroxidase and catalase activities of

FIOMPs are acidic and natural conditions, respectively [27]. In catalase activity, FIOMPs convert H_2O_2 to water and O_2 without consuming additional electron-donor substrates (Eq. 9). In peroxidase activity, they need to a hydrogen donor (HD) to reduce H_2O_2 while generating the oxidized form of HD (Eq. 10) [27,52].

CAT activity $$2H_2O_2 \rightarrow 2\ H_2O + O_2 \quad (9)$$

Peroxidase activity $$H_2O_2 + 2AH \rightarrow 2\ H_2O + 2A \quad (10)$$

Accordingly, FIOMPs could catalyze H_2O_2 to produce hydroxyl radicals in acidic conditions like in lysosomes, and this toxic potential can be a major concern [27]. In general, the intensity of peroxidase activity is highly dependent on the biological environment PH, whether of peroxidase enzyme or the mimetic FIOMPs. In this study, this was not a challenge because of its activity in buffer solution with natural PH = 7, which is almost similar to plasma/blood PH.

The catalytic activity of NPs/MPs is overall dependent on their size. This indicated that the peroxidase-like catalytic activity of Fe_3O_4 nanoparticles is decreased by increasing the NP size [60]. This is contradictory to the lower catalytic activity of FIOMPs compared to CNPs. It is unclear how FIOMPs protect IR-BSA protein similar to the native protein at concentrations of 5–20 mg/L when they can only scavenge H_2O_2 and have a limited catalytic activity. This can be attributed to the mesoporous morphology of FIOMPs. Foley et al. investigated the production and reactivity of hydroxyl radicals in water radiolysis confined to porous materials like controlled pore glasses. The radiolytic yields (in other words, •OH yield) are reduced by decreasing the pore size less than 100 nm. In small pores, the hydroxyl radicals cannot migrate as far apart as in bulk water, and so, regarding to their very short lifetimes, they recombine faster with radicals produced in the same radiolytic track than with a solvent chemical. This phenomenon called “cagelike effect” can also attribute to the porous FIOMPs with nm scale gaps between petals and the reduced intergap encounter probability between the protein and ROS [55]. On the other hand, the presence of FIOMPs in water, due to their micron size, can generally affect ROS diffusion to a greater extent compared to NPs. Thus, the lower catalytic activity of FIOMPs compared to CNPs is compensated by their porous morphology and micron size to scavenge ROS effectively. The cagelike effect and ROS impaired diffusion for water/CNPs is negligible due to their very fine size and no porosity. Because the radio-protectivity of FIOMPs originates more from its morphology than enzyme mimetic activity as a scavenger, it seems that the optimum concentration of irradiated water/FIOMPs system (5–8 mg/L) is greater than that of water/CNPs (2–5 mg/L) to protect BSA effectively. From a pharmaceutical viewpoint, the efficacy of IR-BSA binding to the drug may be improved in the presence CNPs/MFPs compared to the absence of such nano-radioprotectors.

4.5. Toxicity of CNPs/FIOMPs

The toxicity of CNPs/FIOMPs was not evaluated individually in this work due to our focus on the molecular level to obtain preliminary information as a starting point and its extent beyond the purpose of this work. The toxicity results for unique NPs or MPs are completely dependent on physicochemical factors such as size, shape, particle charge, and surface chemistry, as well as the study method, in vitro, or in vivo techniques. Therefore, there is no constant conclusion for unique NPs/MPs and we are highly interested in a comprehensive in vivo study for proposed nanomaterials in the future [61]. However, the correlation between physicochemical parameters and in vitro/in vivo

toxicity of CNPs and iron oxide particles is extensively investigated in the literature. In general, a high surface ratio of NPs is associated with increased toxicity. However, the size-dependent toxicity of NPs is rejected in some studies whereas the MPs and NPs show the same level of toxicity in some [61–62]. The bare or coated surface of NPs/MPs is a very important parameter. Almost all reports have confirmed that bare NPs/MPs have higher toxicity than the coated particles, though some studies have found the toxicity of bare NPs to be less than that of coated ones [61–63]. There are plenty of contradictory results with respect to toxicity for both cerium oxide and iron oxide particles, as can be reported for all NPs [61,64–65]. Thus, the radioprotective properties and toxicity of NPs/MPs are linked substantially to their physicochemical parameters. Hence, a comprehensive study is required to design NPs/MPs while attaining the set goals in both fields (radioprotection and toxicity) simultaneously.

5. Conclusions and future prospects

In this study, the potential radioprotective effects of CNPs and FIOMPs on the structural changes in BSA protein induced by gamma irradiation at a therapeutic dose (3Gy) were investigated. Nanomaterials as an emerging technology have enormous potential for radioprotection as well as in the pathogenesis of various diseases involving oxidative damage induced by ionization radiation. Thus, the structural and functional changes in major proteins like serum albumin irradiated by gamma rays can be considered one of main medical indicators to evaluate the harmful effects in cells/tissues. The pre-irradiation tests by CD and fluorescence spectroscopy showed no significant conformational changes in BSA protein treated with low concentrations of both CNPs and FIOMPs, which encouraged us to study them further. CD and fluorescence measurements showed a loss of protein conformation accompanied with a decrease in the α-helix content, an increase in β-sheets, and random structures, and a decrease in fluorescence emission by gamma irradiation in the absence of NPs. In the presence of both CNPs and FIOMPs, BSA was protected from the structural changes caused by gamma-irradiation. Thus, they possess strong antiradical properties, by scavenging free radicals from water radiolysis. The antioxidant activity, surface chemistry, morphology, confinement arising from porosity, and interfacial phenomena in a heterogeneous system composed of MPs/NPs simultaneously affect the production yield, diffusion (motion), removal, recombination, and mechanisms of ROS production by radiolysis. The radioprotection property of CNPs and FIOMPs is attributed more to enzyme mimetic activities and their porous structure, leading to an increase in ROS recombination with each other in the same radiolytic track, and subsequently decreasing encounters with the BSA protein. Regarding the reasonable functionality of CNPs and FIOMPs, nano-radioprotectors with synergistic effects including strong antioxidant enzyme activity and confinement properties may have more potent radioprotection potential. It can also yield systems with lower optimum concentrations than those reported here, while obtaining less toxicity. We thus are interested to investigate radioprotection activity of porous CNPs like flowers in our future studies. The understanding of all phenomena involved in a heterogeneous system with gamma irradiation is very complex, and requires comprehensive study to find the underlying mechanisms. The complexity and advantages of nano-radioprotectors in comparing the limitations of natural ones are motivating and encouraging for further research in the future. In addition, the safety concerns of nano-radioprotectors must receive substantial consideration in parallel due to their possible side effects on human health. Considering the substantial effect of physicochemical parameters on the radioprotection and toxicity of

NPs/MPs, each of them needs to be quantified in a comprehensive study to eventually produce them as commercial medical drugs. Our results with BSA might be specially generalized to HSA because of 76% sequence homology, as well as with other globular proteins at least for in vitro studies. Regarding the lack of studies on the radioprotective properties of NPs/MPs on the vital proteins in the body, this work may open a new window as a pioneer for future studies.

Acknowledgments

This study was supported by Grants-in-Aid for Scientific Research No. 19H04296 from the Ministry of Education, Culture, Sports, Science and Technology (MEXT), Japanese Government. The authors gratefully acknowledge the use of the services, facilities, and the excellent experimental conditions provided by IBB, Baqiyatallah University of Medical Sciences (Tehran) and the Cyclotron and Radioisotope Center (CYRIC), Tohoku University, Japan.

Conflict of interest

All authors declare no conflicts of interest in this paper.

References

1. Colon J, Hsieh N, Ferguson A, et al. (2010) Cerium oxide nanoparticles protect gastrointestinal epithelium from radiation-induced damage by reduction of reactive oxygen species and upregulation of superoxide dismutase. *Biol Med* 6: 698–705.
2. Kwatra D, Venugopal A, Anant S (2013) Nanoparticles in radiation therapy: a summary of various approaches to enhance radiosensitization in cancer. *Transl Cancer Res* 2: 330–342.
3. Madhu LN, Kumari NS (2014) Radioprotective effect of sulphydryl group containing triazole derivative to modulate the radiation- induced clastogenic effects. *Res in Pharm Sci* 9: 23–29.
4. Borek C (2004) Antioxidants and radiation therapy. *J Nutr* 134: 3207S–3209S.
5. Abdou MI, Abbas OA (2009) Evaluation of diphenyl dimethyl bicarboxylate (DDB) as a probable hepato-protector in rats against whole body gamma irradiation. *Biosci Res* 6: 01–11.
6. Charbonneau D, Beauregard M, Tajmir-Riahi HA (2009) Structural analysis of human serum albumin complexes with cationic lipids. *J Phys Chem* B 113: 1777–1784.
7. Biswas S, Das R, Banerjee ER (2017) Role of free radicals in human inflammatory diseases. *AIMS Biophys* 4: 596–614.
8. Shen L, Tang CH (2012) Microfluidization as a potential technique to modify surface properties of soy protein isolate. *Food Res Int* 48: 108–118.
9. Chen M, Liu Y, Cao H, et al. (2015) The secondary and aggregation structural changes of BSA induced by trivalent chromium: A biophysical study. *J Lumin* 158: 116–124.
10. Yang H, Liu Q, Zhao L, et al. (2014) Fluorescence spectroscopic studies on the interaction of oleanolic acid and its triterpenoid saponins derivatives with two serum albumins. *J Solution Chem* 43: 774–786.
11. Gelamo EL, Silva C, Imasato H, et al. (2002) Interaction of bovine (BSA) and human (HSA) serum albumins with ionic surfactants: spectroscopy and modelling. *BBA-Protein Struct Mol Enzymol* 1594: 84–99.

12. Gaber MH (2005) Effect of γ-irradiation on the molecular properties of bovine serum albumin. *J Biosci Bioeng* 100: 203–206.
13. Khorolskyi OV, Malomuzh NP (2020) Macromolecular sizes of serum albumins in its aqueous solutions. *AIMS Biophys* 7: 219–235.
14. Chudzik M, Maciążek-Jurczyk M, Pawełczak B, et al. (2016) Spectroscopic studies on the molecular ageing of serum albumin. *Molecules* 22: 34.
15. Schuessler H, Schilling K (1984) Oxygen effect in the radiolysis of proteins: Part 2 bovine serum albumin. *Inter J Radiat Biol Relat Stud Phys, Chem Med* 45: 267–281.
16. Hu X, Song W, Li W, et al. (2016) Effects of γ-irradiation on the molecular structures and functions of human serum albumin. *J Biochem Mol Toxic* 30: 525–532.
17. Zarei H, Bahreinipour M, Eskandari K, et al. (2017) Spectroscopic study of gamma irradiation effect on the molecular structure of bovine serum albumin. *Vacuum* 136: 91–96
18. Noroozi M, Angerson WJ, Lean ME (1988) Effects of flavonoids and vitamin C on oxidative DNA damage to human lymphocytes. *Am J Clin Nutr* 67: 1210–1218.
19. Kumar B, Jha MN, Cole WC, et al. (2002) D-alpha-tocopheryl succinate (vitamin E) enhances radiation-induced chromosomal damage levels in human cancer cells, but reduces it in normal cells. *J Am Coll Nutr* 21: 339–343.
20. Mishra K, Ojha H, Kallepalli S, et al. (2014) Protective effect of ferulic acid on ionizing radiation induced damage in bovine serum albumin. *Int J Radiat Res* 12: 113.
21. Abdel Fattah SM, Fahim TM, El-Fatih NM (2011) Prophylactic role of combined treatment with wheat germ oil and ginseng against radiation injury in male rats. *Egypt J Hosp Med* 45: 403–415.
22. Verma S, Gupta ML, Dutta A, et al. (2010) Modulation of ionizing radiation induced oxidative imbalance by semi-fractionated extract of Piper betel: an in vitro and in vivo assessment. *Oxid Med Cell Longev* 3: 44–52.
23. Ferreira CA, Ni D, Rosenkrans ZT, et al. (2018) Scavenging of reactive oxygen and nitrogen species with nanomaterials. *Nano Res* 11: 4955–4984.
24. Singh S (2019) Nanomaterials exhibiting enzyme-like properties (Nanozymes): Current advances and future perspectives. *Front Chem* 7: 46.
25. Colon J, Herrera L, Smith J, et al. (2009) Protection from radiation-induced pneumonitis using cerium oxide nanoparticles. *Nanomed: Nanotechnol* 5: 225–231.
26. Tarnuzzer RW, Colon J, Patil S, et al. (2005) Vacancy engineered ceria nanostructures for protection from radiation-induced cellular damage. *Nano Lett* 5: 2573–2577.
27. Chen Z, Yin JJ, Zhou YT, et al. (2012) Dual enzyme-like activities of iron oxide nanoparticles and their implication for diminishing cytotoxicity. *ACS Nano* 6: 4001–4012.
28. Wei H, Wang E (2008) Fe_3O_4 magnetic nanoparticles as peroxidase mimetics and their applications in H_2O_2 and glucose detection. *Anal Chem* 80: 2250–2254.
29. Liu X, Wei W, Yuan Q, et al. (2012). Apoferritin-CeO_2 nano-truffle that has excellent artificial redox enzyme activity. *Chem Commun* 48: 3155–3157.
30. Zhong LS, Hu JS, Liang HP, et al. (2006) Self-Assembled 3D flowerlike iron oxide nanostructures and their application in water treatment. *Adv Mater* 18: 2426–2431.
31. Chi Z, Liu R (2011) Phenotypic characterization of the binding of tetracycline to human serum albumin. *Biomacromolecules* 12: 203–209.

32. Pignataro MF, Herrera MG, Dodero VI (2020) Evaluation of peptide/protein self-assembly and aggregation by spectroscopic methods. *Molecules* 25: 4854.
33. Le Caër S (2011) Water radiolysis: influence of oxide surfaces on H_2 production under ionizing radiation. *Water* 3: 235–253.
34. Uygun-Sarıbay M, Ergun E, Kalaycı Y, et al. (2017) The secondary structure of proteins in liquid, frozen, and dried egg-white samples: Effect of gamma irradiation treatment. *Int J Food Prop* 20: 1195–1203.
35. Zolghadri S, Saboury AA, Amin E, et al. (2010) A spectroscopic study on the interaction between ferric oxide nanoparticles and human hemoglobin. *J Iran Chem Soc* 7: S145–S153.
36. Hollóczki O, Gehrke S (2019) Nanoplastics can change the secondary structure of proteins. *Sci Rep* 9: 1–7.
37. Gopinath PM, Saranya V, Vijayakumar S, et al. (2019) Assessment on interactive prospectives of nanoplastics with plasma proteins and the toxicological impacts of virgin, coronated and environmentally released-nanoplastics. *Sci Rep* 9: 8860.
38. Ray D, Paul BK, Guchhait N (2012) Effect of biological confinement on the photophysics and dynamics of a proton-transfer phototautomer: an exploration of excitation and emission wavelength-dependent photophysics of the protein-bound drug. *Phys Chem Chem Phys* 14: 12182–12192.
39. Wang Y, Zhang H, Kang Y, et al. (2016) Effects of perfluorooctane sulfonate on the conformation and activity of bovine serum albumin. *J Photoch Photobio B: Biol* 159: 66–73.
40. Pal S, Pyne P, Samanta N, et al. (2020) Thermal stability modulation of the native and chemically-unfolded state of bovine serum albumin by amino acids. *Phys Chem Chem Phys* 22: 179–188.
41. Pant MP, Mariam J, Joshi A, et al. (2014) UV radiation sensitivity of bovine serum albumin bound to silver nanoparticles. *J Radiat Res Appl Sci* 7: 399–405.
42. Lu JQ, Jin F, Sun TQ, et al. (2007) Multi-spectroscopic study on interaction of bovine serum albumin with lomefloxacin–copper (II) complex. *Int J Biol Macromol* 40: 299–304.
43. Borowska M, Mylkie K, Nowak P, et al. (2020) Testing for ketoprofen binding to HSA coated magnetic nanoparticles under normal conditions and after oxidative stress. *Molecules* 25: 1945.
44. Nasir I, Lundqvist M, Cabaleiro-Lago C (2015) Size and surface chemistry of nanoparticles lead to a variant behavior in the unfolding dynamics of human carbonic anhydrase. *Nanoscale* 7: 17504–17515.
45. Gagner JE, Lopez MD, Dordick JS, et al. (2011) Effect of gold nanoparticle morphology on adsorbed protein structure and function. *Biomaterials* 32: 7241–7252.
46. Wu X, Narsimhan G (2008) Effect of surface concentration on secondary and tertiary conformational changes of lysozyme adsorbed on silica nanoparticles. *BBA-Proteins Proteom* 1784: 1694–1701.
47. Chetty R, Singh M (2020) In-vitro interaction of cerium oxide nanoparticles with hemoglobin, insulin, and dsDNA at 310.15 K: Physicochemical, spectroscopic and in-silico study. *Int J Biol Macromol* 156: 1022–1044.
48. Shemetov AA, Nabiev I, Sukhanova A (2012) Molecular interaction of proteins and peptides with nanoparticles. *ACS Nano* 6: 4585–4602.
49. Litvinov RI, Faizullin DA, Zuev YF, et al. (2012) The α-helix to β-sheet transition in stretched and compressed hydrated fibrin clots. *Biophys J* 103: 1020–1027.

50. Wei YS, Lin SY, Wang SL, et al. (2003) Fourier transform IR attenuated total reflectance spectroscopy studies of cysteine-induced changes in secondary conformations of bovine serum albumin after UV-B irradiation. *Biopolymers* 72: 345–351.
51. Salvia A, Carrupta PA, Tillement JP, et al. (2001) Structural damage to proteins caused by free radicals: asessment, protection by antioxidants, and influence of protein binding. *Biochem Pharmacol* 61: 1237–1242.
52. Gao L, Fan K, Yan X (2020) Iron oxide nanozyme: A multifunctional enzyme mimetics for biomedical application, *Nanozymology*, Singapore: Springer, 105–140.
53. Singh S (2019) Nanomaterials exhibiting enzyme-like properties (Nanozymes): Current advances and future perspectives. *Front Chem* 7: 46.
54. Korsvik C, Patil S, Seal S, et al. (2007) Superoxide dismutase mimetic properties exhibited by vacancy engineered ceria nanoparticles. *Chem Commun* 10: 1056–1058.
55. Foley S, Rotureau P, Pin S, et al. (2005) Radiolysis of confined water: production and reactivity of hydroxyl radicals. *Angew Chem Int Edit* 44: 110–112.
56. Rotureau P, Renault JP, Lebeau B, et al. (2005) Radiolysis of confined water: molecular hydrogen formation. *ChemPhysChem* 6: 1316–1323.
57. Singh R, Singh S (2015) Role of phosphate on stability and catalase mimetic activity of cerium oxide nanoparticles. *Colloid Surface B* 132: 78–84.
58. Schlick S, Danilczuk M, Drews AR, et al. (2016) Scavenging of hydroxyl radicals by ceria nanoparticles: effect of particle size and concentration. *J Phys Chem C* 120: 6885–6890.
59. Xue Y, Luan Q, Yang D, et al. (2011) Direct evidence for hydroxyl radical scavenging activity of cerium oxide nanoparticles. *J Phys Chem C* 11: 4433–4438.
60. Peng FF, Zhang Y, Gu N (2008) Size-dependent peroxidase-like catalytic activity of Fe_3O_4 nanoparticles. *Chinese Chem Lett* 19: 730–733.
61. Patil US, Adireddy S, Jaiswal A, et al. (2015) In vitro/in vivo toxicity evaluation and quantification of iron oxide nanoparticles. *Int J Mol Sci* 16: 24417.
62. Kumari M, Singh SP, Chinde S, et al. (2014) Toxicity study of cerium oxide nanoparticles in human neuroblastoma cells. *Int J Toxicol* 33: 86–97.
63. Demokritou P, Gass S, Pyrgiotakis G, et al. (2013) An in vivo and in vitro toxicological characterization of realistic nanoscale CeO_2 inhalation exposures. *Nanotoxicology* 7: 1338–1350.
64. Gagnon J, Fromm KM (2015) Toxicity and protective effects of cerium oxide nanoparticles (nanoceria) depending on their preparation method, particle size, cell type, and exposure route. *Eur J Inorg Chem* 27: 4510–4517.
65. Leung YH, Yung MMN, Ng AMC, et al. (2015) Toxicity of CeO_2 nanoparticles–The effect of nanoparticle properties. *J Photochem Photobiol B: Biol* 145: 48–59.